JOURNAL OF MULTIFUNCTIONAL MATERIALS & PHOTOSCIENCE
12(1), June 2021, pp. 95-113

# Research progress of indium sulfide-based semiconductor regulation and photocatalytic performance

**Chao Liu[a], Fengjun Zhang[a,b*], Chunmei Kai[a], Weiqin Cai[a], Cui Kong[a]**
[a]*Key Laboratory of Functional Molecule Design and Interface Process, Anhui Jianzhu University, Hefei Anhui, 230601, P. R. China.*
[b]*Anhui Key Laboratory of Advanced Building Materials, Anhui Jianzhu University, Hefei Anhui, 230022, P. R. China.*

***Abstract***: With the development, environmental problems and energy shortages have become increasingly prominent. Photocatalysis is an ideal way to solve these two problems. $In_2S_3$ is a highly efficient semiconductor material, which has attracted wide attention because of its suitable band gap (2.0eV-2.2eV), good light absorption ability, good electron migration ability and low toxicity. However, $In_2S_3$ itself has some other problems, such as the photo-corrosion condition in the photocatalytic process and the photocatalytic hydrogen evolution performance of pure indium sulfide is not particularly excellent. This article mainly introduces the crystal structure of $In_2S_3$. $In_2S_3$ was prepared by different methods, and the morphology was adjusted to optimize the photocatalytic performance of $In_2S_3$. In addition, the photocatalytic degradation and hydrogen production ability of $In_2S_3$ was enhanced by forming a heterojunction.

**Keywords:** $In_2S_3$; morphology control; heterojunction; photocatalysis; degradation; hydrogen production

## 1. Introduction

Nowadays, the increasingly serious environmental pollution and the globalization of the energy crisis have attracted more and more attention [1, 2]. The method of using solar energy to split water to produce hydrogen by photocatalysis on semiconductors is one of the most effective ways to obtain clean and recyclable energy to replace traditional fossil fuels[3, 4]. Since the 1870s, Japanese scientists Fujishima and Honda discovered that n-type semiconductor $TiO_2$ can decompose water to obtain hydrogen under external radiation[5], Photocatalytic hydrogen production has been deeply studied by researchers in related fields. But $TiO_2$ itself has many shortcomings, its band gap is 3.2eV [6]ÿit can only absorb light in the ultraviolet region (<400nm). But ultraviolet light only accounts for 5% of sunlight, and visible light (400nm~780nm) accounts for 47% of the sun's largest proportion[7]. The light-absorbing ability of light mainly depends on their band

* Corresponding author*: fjzhang@ahjzu.edu.cn*

gap[8]. Therefore, synthesizing a narrow band gap visible light-responsive semiconductor photocatalyst is the current research direction in the field of photocatalysis.

With the in-depth research in the field of photocatalysis, people have discovered that metal sulfides are a potential semiconductor material, and they have a suitable narrow band gap[9, 10].Therefore, it can absorb visible light and has a strong absorption capacity in the visible light region. As a kind of III-IV group semiconductor compound, $In_2S_3$ has a band gap of 2.0eV-2.2eV[11, 12]. Like other metal sulfides, $In_2S_3$ has suitable band gap width, suitable band gap position, exposed active sites, high light energy utilization, chemical stability and strong photocatalytic activity [9, 13-15]. Compared with other toxic metal sulfide semiconductors (CdS), $In_2S_3$ is almost non-toxic [16].

This article mainly introduces the five different crystal types of $In_2S_3$, such as defect cubic structure, defect spinel structure, layered hexagonal structure, phase rhomboid structure, phase cubic defect structure, and distinguish different morphological features through different dimensions ; Use a variety of methods such as chemical bath deposition, hydrothermal, solvothermal and chemical vapor deposition to prepare $In_2S_3$, and combine it with other semiconductors to form different heterojunctions (such as: type I, type II, p-n type , Z-type heterojunction) to enhance the hydrogen production efficiency of $In_2S_3$ photocatalyst.

## 2. Preparation and Experimental procedures

$In_2S_3$ has five crystal forms. Under standard atmospheric pressure, $\alpha$-$In_2S_3$ with defective cubic structure, $\beta$-$In_2S_3$ with defective spinel structure and $\gamma$-$In_2S_3$ with layered hexagonal structure can be prepared under standard atmospheric pressure. These three different crystals, the structure mainly depends on different temperatures [17-19]. Figure 1 is the crystal structure diagram of the above three $In_2S_3$[20]. Below 420°C, the tetragonal $\beta$-$In_2S_3$ can maintain a stable structure. When it exceeds 420°C, the tetragonal $\beta$-$In_2S_3$ will transform into cubic $\beta$-$In_2S_3$ and cubic $\alpha$-$In_2S_3$. The layered hexagonal structure of $\gamma$-$In_2S_3$ appears above 750°C. Under high pressure, $\varepsilon$-$In_2S_3$ with phase rhomboid structure and $Th_3P_4$-$In_2S_3$ with phase cubic defect structure can be prepared[21]. Among the above five different crystal structure types of $In_2S_3$, $\beta$-$In_2S_3$ is the only n-type semiconductor among the three stable $In_2S_3$ crystal states[11, 22, 23], it has a cubic or tetragonal structure[24], because of its stable chemical properties at room temperature and strong visible light Absorptive capacity and low toxicity tend to attract the attention of scientific researchers[25].

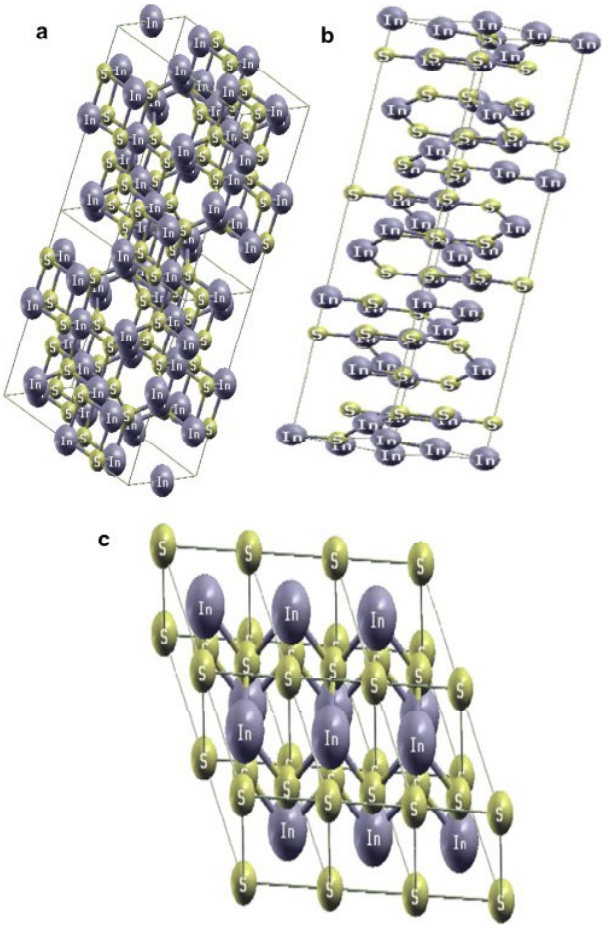


Figure 1 (a) The cubic crystal structure defect of the unit cell of $\alpha$ -$In_2S_3$; (b) The tetragonal crystal structure defect of the unit cell of $\beta$ -$In_2S_3$; (c) The triangular crystal structure of the unit cell of $\gamma$ -$In_2S_3$ [20]

Different preparation methods will have a certain impact on the physical and chemical properties of the material, so it is very important to choose a suitable method to prepare the required material. $In_2S_3$ preparation methods include chemical bath deposition, hydrothermal, solvothermal and chemical vapor deposition.

Chemical bath deposition method: The chemical bath deposition method is a chemical reduction process that uses a suitable reducing agent to reduce metal ions in the plating solution and deposits on the surface of the substrate. It is usually used to prepare metal sulfide films. This reaction usually occurs between dissolved precursors in a low-temperature aqueous solution. C.D. Lokhande et al [26] reported a method for preparing $In_2S_3$ thin films by chemical bath deposition. In this synthesis method, the synthesis effect of the $In_2S_3$ film is affected by the concentration ratio of indium and sulfide ions and the temperature. High-quality $In_2S_3$ film can be obtained when the molar ratio of indium ion to sulfide ion reaches 1:5 and the temperature is 50!-70!.

Hydrothermal method: Hydrothermal method refers to a method in which powder is dissolved in water and recrystallized under high temperature and high pressure in a specific sealed environment. Under subcritical and supercritical hydrothermal conditions, since the reaction is at the molecular level, the reactivity is high. The hydrothermal method can be traced back to geologists' research on simulating mineralization in nature in the middle of the 19th century. After 1900, scientists established the theory of hydrothermal synthesis, and then began to study functional materials. The hydrothermal method has the advantages of low cost, simple operation, and easy control of reaction conditions. It is also one of the good methods for preparing $In_2S_3$. Cui et al [27] combined $In_2S_3$ and $Bi_2MoO_6$ by hydrothermal method to form a heterojunction. The type of heterojunction formed after measurement was type a!. The existence of $In_2S_3$ made the $In_2S_3/Bi_2MoO_6$ heterojunction absorb sunlight. Compared with $Bi_2MoO_6$, it has a significant red shift and a stronger response to photocurrent, which helps to enhance the photocatalytic activity of the composite heterostructure. Fu et al [28] also used the hydrothermal method to simultaneously prepare the tetragonal (T-$In_2S_3$) and cubic (C-$In_2S_3$) â-$In_2S_3$, and found T-$In_2S_3$ with better crystallinity and stronger visible light absorption. C-$In_2S_3$, which has no photocatalytic hydrogen production activity but relatively poor crystallinity and weak visible light absorption, has stable activity. This phenomenon is attributed to the fact that T-$In_2S_3$, which has ordered indium cation vacancies, is further affected by photogenerated electron migration than that which is solely affected by indium ion vacancies.

The solvothermal method is similar to the hydrothermal method. It is a synthetic method in which organic solvents or non-aqueous solvents are reacted at a certain temperature and pressure. It differs from the hydrothermal method in that the solvent used is organic instead of water. Liu et al [29] reported an ultra-thin β-$In_2S_3$ nanotube prepared by solvothermal method. The outer diameter of the nanotube is 10-20nm, the wall thickness is about 2nm, and the length is greater than 1μm. Compared with the bulk $In_2S_3$, the ultraviolet absorption band of the prepared nanotube $In_2S_3$ has a blue shift.

Chemical vapor deposition is an effective preparation method for preparing metal sulfides. In the preparation process, the reactants are first vaporized, and then transferred to the deposition area, and finally chemical reactions are carried out on specific materials to produce the required Material method. Hang et al [30] reported a method for preparing two-dimensional $In_2S_3$ nanosheets by chemical vapor deposition for the first time. Compared with one-dimensional $In_2S_3$ nanowires prepared by chemical vapor deposition, two-dimensional $In_2S_3$ nanosheets are more suitable for manufacturing complex structural components. The advantage of chemical vapor deposition method is that it can obtain higher purity two-dimensional $In_2S_3$ nanosheets, and the prepared nanosheets have a wide range of light response from visible light to near infrared.

Adjusting the morphology of $In_2S_3$ is an effective way to improve its photocatalytic hydrogen evolution ability, as shown in Figure 2, according to the different morphology and structure , $In_2S_3$ can be divided into zero-dimensional structure (E.g: Nanoparticles

[31, 32])ÿOne-dimensional structure (E.g: Nanowires [33-35], Nano stave [36], Nanotube ÿÿTwo-dimensional structure (E.g: Nanosheets [37, 38]) and three-dimensional structure (E.g: Nano flower [39-41]ÿHollow microspheres [42, 43]

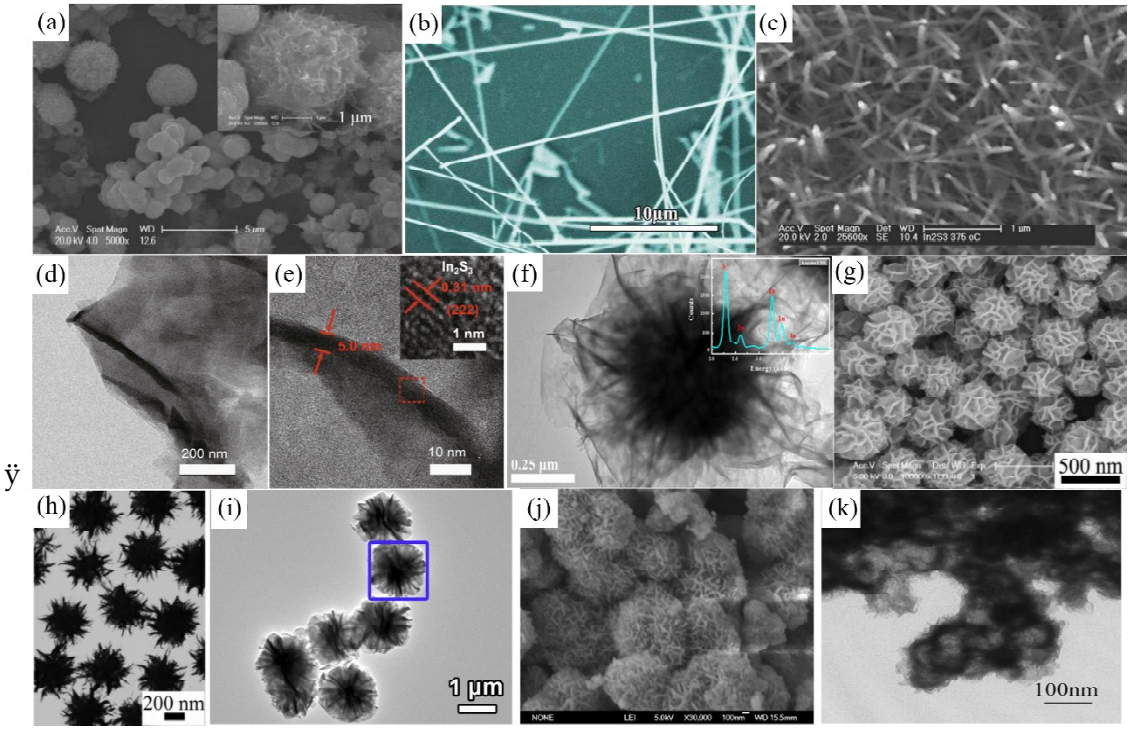


Figure 2 (a) SEM image of $In_2S_3$ nanoparticles [31]; (b) SEM image of $In_2S_3$ nanowire [33]; (c) SEM image of $In_2S_3$ nanorods [36]; (d-e) TEM image and HRTEM image of $In_2S_3$ nanosheet [38]; (f) TEM image of $In_2S_3$ nanoflower [39] (g-h) SEM and TEM images of $In_2S_3$ nanoflowers [40]; (g-h) SEM and TEM images of $In_2S_3$ nanoflowers [41] ; (J-k) FESEM and TEM images of $In_2S_3$ hollow microspheres [42]

## 3. Results and discussion

### *3.1 0 D $In_2S_3$*

Zero-dimensional structure refers to a material whose three dimensions are all in the nanometer size (1-100nm). Because surface atoms account for a large proportion, the surface state density of the structure is greatly increased, so the influence of various quantum effects is very significant.

Zhang et al [32] used continuous ion layer adsorption and reaction to prepare $In_2S_3$ nanoparticles by depositing $In_2S_3$ nanoparticles on $TiO_2$ nanotubes to obtain $In_2S_3/TiO_2$ composites. Through diffuse reflectance spectroscopy, it is found that compared with pure $TiO_2$ nanotubes, the $In_2S_3/TiO_2$ heterostructure shows an excellent visible light response, which is stronger in the visible light region and improves the utilization of sunlight. And the photocurrent density is significantly increased, indicating that the transfer of photogenerated electrons is faster. Xia et al [31] used a simple hydrothermal

synthesis method to grow $In_2S_3$ nanoparticles in situ on graphene as a growth substrate. The prepared graphene/$In_2S_3$ composite material is used for the anode of the battery and has better cycle life and cycle stability. The prepared GIS composite material can still maintain a certain capacity of about 1000mV h $g^{-1}$ after being recycled for more than 200 times. The composite of graphene and $In_2S_3$ also significantly improved the morphology and phase stability of $In_2S_3$.

### *3.2 1 D In2S3*

One-dimensional materials generally refer to linear materials in which atoms are regularly arranged to the order of centimeters in one direction and few atoms are arranged in the other two directions. One-dimensional materials have great application prospects and utilization values in nanomaterials, and they play a key role in nanoelectronics and optical devices. One-dimensional structures also have good effects in the field of photocatalysis.

Afzaal et al [36] reported for the first time that an $In_2S_3$ film composed of $In_2S_3$ nanorods was prepared by using $[Et_2In(S_2CNMe^nBu)]$ as a precursor and using aerosol-assisted chemical vapor deposition to avoid the generation of high temperature and toxic substances. The preparation of one-dimensional $In_2S_3$ nanorods has opened up a new path.

### *3.3 2 D $In_2S_3$*

Two-dimensional materials refer to materials in which electrons can only move freely on the nanometer scale in two dimensions of 1-100nm [44].Two-dimensional materials have a large specific surface area and can provide more active sites, thereby enhancing the ability of photocatalytic hydrogen production. If the nanoparticles are combined with the two-dimensional photocatalyst, the agglomeration of the nanoparticles can be avoided, which is conducive to the transfer of charges, which helps to improve the activity and stability of the photocatalyst [45].

Chen et al [37] reported a one-step solvothermal method to prepare a composite photocatalyst composed of $Bi_2S_3$ nanoflowers and $In_2S_3$ nanosheets. This synthesis is based on the different growth rates of these two sulfides. The relatively slow-growing ultra-thin $In_2S_3$ is formed by the relatively fast-growing $Bi_2S_3$ as the growth substrate. The introduction of $In_2S_3$ greatly improves the light absorption capacity of the $Bi_2S_3$/ $In_2S_3$ complex, increases the charge transfer rate, and improves the effective separation of electron-hole pairs, which makes its photocatalytic activity compared to pure $In_2S_3$ and pure $In_2S_3$. The $Bi_2S_3$ has been greatly improved, and the stability of its photocatalytic activity after several cycles has also been enhanced.

Li et al [38] used the atomic layer deposition method to uniformly wrap ZnO in the sheet-like $In_2S_3$ to form a core-shell structured $In_2S_3$/ZnO composite. The optical properties of $In_2S_3$/ZnO can be controlled by adjusting the thickness of the coated ZnO. When the thickness of ZnO reaches 50nm, $In_2S_3$/ZnO presents the best appearance.

Compared with the $In_2S_3$ nanosheet array without ZnO, the $In_2S_3$/ZnO composite exhibits stronger light absorption capacity and is accompanied by a red shift of the absorption peak. The photocurrent density and incident photocurrent efficiency at 380nm are also 70 and 160 times that of the original $In_2S_3$ nanosheet array, respectively. The II heterojunction structure formed by $In_2S_3$ and ZnO is also the reason for improving the transfer and separation of photogenerated carriers.

### *3.4 3 D $In_2S_3$*

Three-dimensional nanostructure refers to a composite material composed of one or more basic structural units in zero-dimensional, one-dimensional, and two-dimensional[46]. Electrons can move freely in three non-nano-sized dimensions, and usually have a relatively regular morphology and a relatively large specific surface area.

Chen et al [40] used indium chloride and L-cysteine as indium source and sulfur source to synthesize a highly dispersed cubic flower-like $In_2S_3$ assembled from nanosheets through self-assembly. The diameter of the prepared flower-shaped $In_2S_3$ is about 400nm, and the thickness of the $In_2S_3$ nanoflake of the structure is about 10nm. Adjusting the pH of the solution during the preparation process will also affect the morphology and structure of $In_2S_3$. $In_2S_3$ that has not been adjusted for pH will form larger particles, and an excessively large pH value will cause $In_2S_3$ to have more flower-like patterns. The scattered, it is difficult to gather. The ultra-high specific surface area of $In_2S_3$ and the mid-frequency absorption range of visible light may bring development to the direction of photocatalysis.

Liu et al [42] prepared a cubic phase β -$In_2S_3$ with a hollow nano-spherical morphology structure by a two-step solvothermal method, with an outer diameter of 70nm and a shell thickness of 20nm. After UV diffuse reflectance and PL tests, it is found that the peak position of bulk $In_2S_3$ on the market shifts to the UV region. It can be explained as the quantum confinement effect of the hollow nano-spherical morphology on β -$In_2S_3$.

### *3.5 Indium sulfide-based semiconductor heterojunction*

Indium sulfide is very suitable as a semiconductor material for photocatalytic hydrogen evolution because of its suitable band gap width and suitable band gap position. The bottom of the conduction band in pure $In_2S_3$ is at -0.8V, which is more negative than the redox potential of $H^+$ at 0V [47], the top of the valence band is located at 1.5V, which is slightly positive compared to the redox potential of $O_2$. This makes the band gap position of $In_2S_3$ sufficient to ensure that water can be split to produce hydrogen [21]. When applied to photocatalytic degradation, the position of the valence band or conduction band of the semiconductor is more positive or negative relative to the redox potential of the pollutant to be degraded.

There are many ways to improve the photocatalytic activity of semiconductor photocatalysts, such as morphology control, crystal plane control, element doping, dye sensitization, and semiconductor recombination. Among them, the method of

compounding with a semiconductor to construct a heterojunction is a feasible and most commonly used method to improve the performance of $In_2S_3$. In particular, the charge separation efficiency can be enhanced by a heterostructure. There are four types of reported $In_2S_3$-based photocatalytic heterojunctions. Types: type I, type II, p-n type and Z type heterojunction.

### *3.6 $In_2S_3$-based type I heterojunction*

For type I semiconductors (as shown in Figure 3), the conduction band and valence band positions of semiconductor A are higher and lower than those of semiconductor B, respectively. Therefore, the electrons and holes of semiconductor A under light irradiation They are all transferred to the conduction band and valence band of semiconductor B. Electrons and holes gather on the same semiconductor at the same time, which also leads to easier recombination of electrons and holes[48].

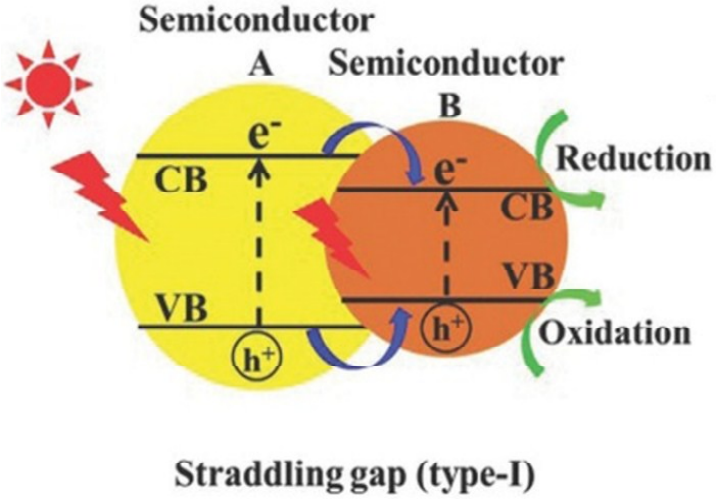


Figure 3: Type I semiconductor [48]

Ma et al [49] reported a new type of transition metal carbide $Mo_2C$ and $In_2S_3$ composite photocatalyst prepared by hydrothermal method. The composite of $Mo_2C$ and $In_2S_3$ forms a type I heterojunction (as shown in Figure 4a). When the content of $Mo_2C$ reaches 30%, the maximum hydrogen production performance of $Mo_2C/In_2S_3$ nanocomposites is 535.58 $\mu mol \cdot h^{-1} \cdot g^{-1}$, which is 175.6 times of the original pure $In_2S_3$. When $Mo_2C$ and Pt account for 1% of $In_2S_3$, the $Mo_2C/In_2S_3$ composite also has 2.68 times higher photocatalytic hydrogen production performance than the $Pt/In_2S_3$ composite. It is not difficult to see from the PL diagram (Figure 4b) that this result can be attributed to the sheet-to-sheet structure providing more or active sites for the transfer of photogenerated electrons and the type I heterogeneity composed of $Mo_2C$ and $In_2S_3$. Mass junction reduces the recombination rate of electron-hole pairs.

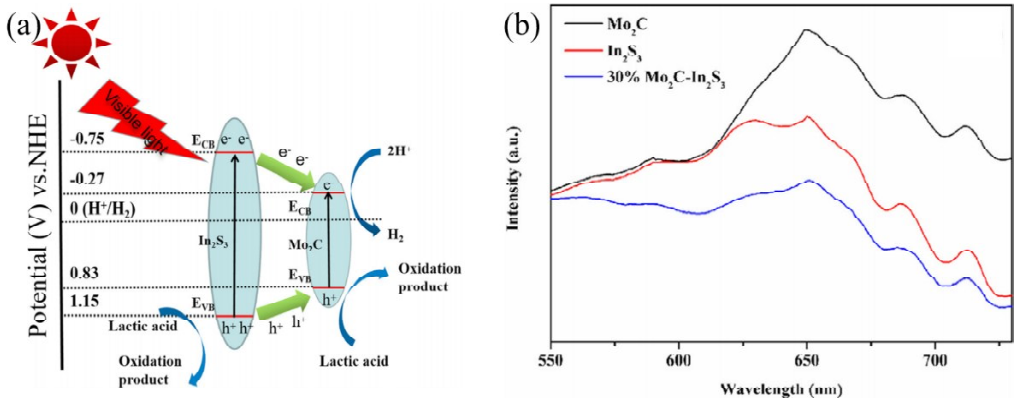


Figure 4: (a) $Mo_2C/In_2S_3$ electron migration and separation mechanism diagram; (b) $In_2S_3$, $Mo_2C$ and $Mo_2C$-$In_2S_3$ heterojunction photocatalysts photoluminescence spectra at an excitation wavelength of 350 nm [49]

Yang et al [50] reported a simple hydrothermal process to synthesize type I core-shell $In_2O_3/In_2S_3$ nanostructures under mild conditions (Figure 5a). Adjust the amount of $In_2S_3$ compared to $In_2O_3$ by changing the hydrothermal temperature. When the temperature is controlled at 60°C and 90°C (as shown in Figure 5b), the $In_2S_3$ content increases with the increase in temperature. When the hydrothermal temperature reaches 120°C When $In_2O_3$ is completely converted to $In_2S_3$. When the temperature is 90!, the effect of $In_2O_3/In_2S_3$ hydrogen evolution of vegetation is the best.

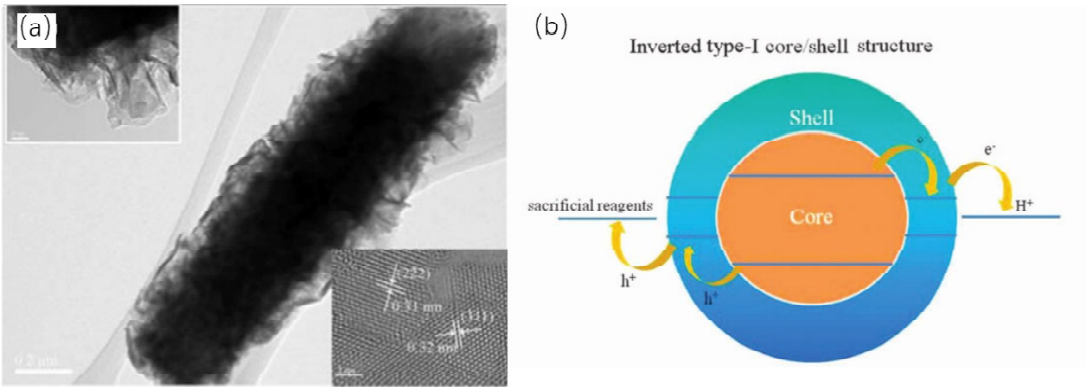


Figure 5: (a) TEM image of the core-shell structure of $In_2O_3/In_2S_3$ obtained at 90°C; (b) Schematic diagram of the band gap position of the I-type core-shell structure [50]

### *3.7 $In_2S_3$ base type a! heterojunction*

For type II heterojunction (Figure 6), the conduction band position of semiconductor A is higher than that of semiconductor B, and the valence band position of semiconductor B is lower than that of semiconductor B. This results in the accumulation of electrons and holes. Semiconductors, so compared to type I semiconductors, type II semiconductors can better realize the separation of electrons and holes [48].

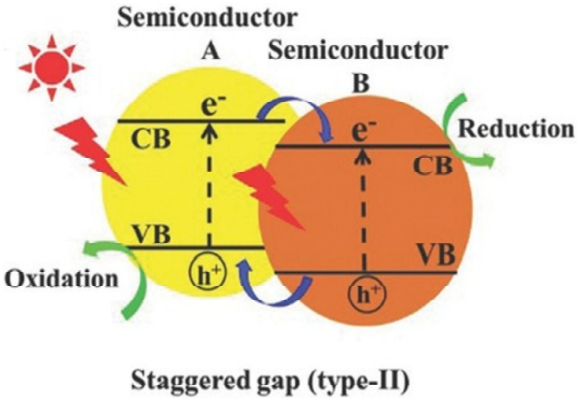


Figure 6: Type a! heterojunction [48]

Liu et al.[51] used a simple in-situ oxidation method to prepare a hydrangea-like $In_2S_3$/$In_2O_3$ photocatalyst with layered voids (Figure 7a). The $In_2S_3$/$In_2O_3$ heterostructure obtained by annealing the $In_2S_3$ prepared by hydrothermal method at 450! has the highest photocatalytic activity, and the hydrogen generation rate reaches 683.8 μmol·$g^{-1}$ after 5 hours of irradiation. Compared with pure $In_2S_3$ and pure $In_2O_3$, the photocatalytic performance is increased by 2.56 times and 3.48 times, respectively (Figure 7b), Liu obtained the bandgap width of $In_2S_3$ and $In_2O_3$ from the absorption spectrum according to the Kubelka-Munk equation, where the band gap width of $In_2S_3$ is 2.16 eV, and the band gap width of $In_2O_3$ is 3.09eV. XPS valence spectroscopy measured the valence band widths of $In_2S_3$ and $In_2O_3$ to be 1.32V and 2.35V, respectively. $In_2S_3$ and $In_2O_3$ form a type II heterojunction, and the electrons in the conduction band of $In_2S_3$ are transferred to $In_2O_3$, the holes in the valence band of $In_2O_3$ are transferred to $In_2S_3$ (Figure 7c). This greatly promotes the separation of charges and holes and reduces the recombination of electron-hole pairs.

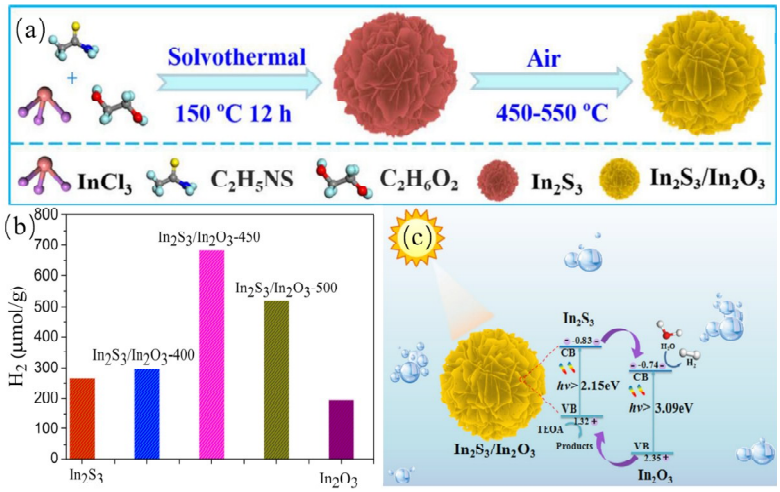


Figure 7: (a) Synthesis process of $In_2S_3$/$In_2O_3$ heterostructure; (b) $In_2S_3$, $In_2O_3$ and $In_2S_3$/$In_2O_3$ samples annealed at different temperatures for photocatalytic hydrogen desorption; (c) $In_2S_3$/$In_2O_3$ heterojunction photocatalysis Schematic diagram of hydrogen escape mechanism [51]

Dan et al [52] successfully prepared $In_2S_3$/CuS metal sulfide composite material by hydrothermal method. $In_2S_3$ and CuS form a type II heterojunction (Figure 8a). The photocatalytic hydrogen production efficiency of $In_2S_3$/CuS composite material can reach 14950 μmol·g$^{-1}$·h$^{-1}$ (Figure 8b). The combination of $In_2S_3$ and CuS improves the light absorption ability of the composite material and promotes the separation ability of photogenerated carriers.

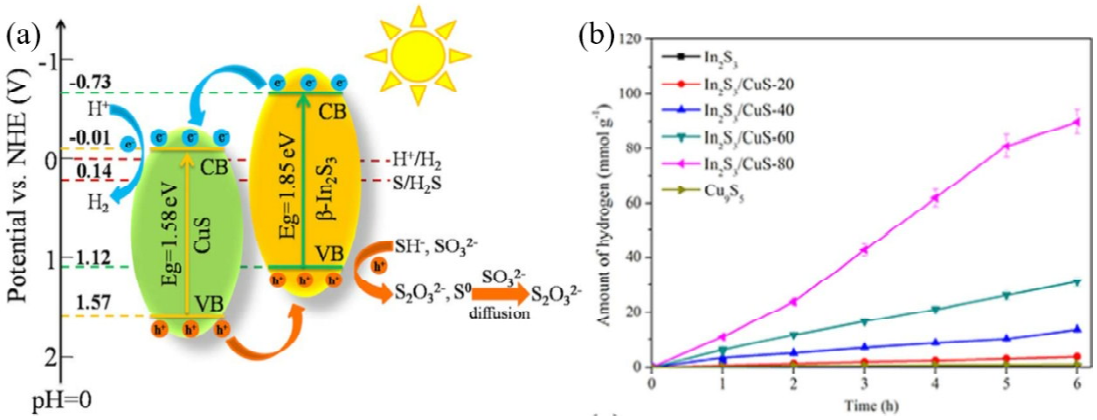


Figure 8: (a) Photocatalytic process of $In_2S_3$/CuS composite material splitting $H_2S$ under visible light irradiation; (b) Photocatalytic hydrogen generation rate of these samples under visible light irradiation [52]

### *3.8 $In_2S_3$-based p-n heterojunction*

This type of heterojunction is composed of a p-type semiconductor and an n-type semiconductor compound (Figure 9). Before being exposed to light, at the contact surface of the two semiconductors, the electrons on the n-type semiconductor diffuse to the p-type semiconductor, and the holes on the p-type semiconductor diffuse to the n-type semiconductor until the system reaches the Fermi level balance. At this time, a built-in electric field is formed at the contact surface. When exposed to light, the p-type and n-type semiconductors obtain sufficient energy, and the electrons are excited from the valence band position to the conduction band position, and due to the existence of the built-in electric field, the electrons gathered at the conduction band position of the p-type semiconductor and the valence band position of the n-type semiconductor The accumulated holes are accelerated to transfer the conduction band position of the n-type semiconductor and the valence band position of the p-type semiconductor. Compared with type II and type I heterojunctions, p-n type heterojunctions have stronger electron-hole separation ability[48] .

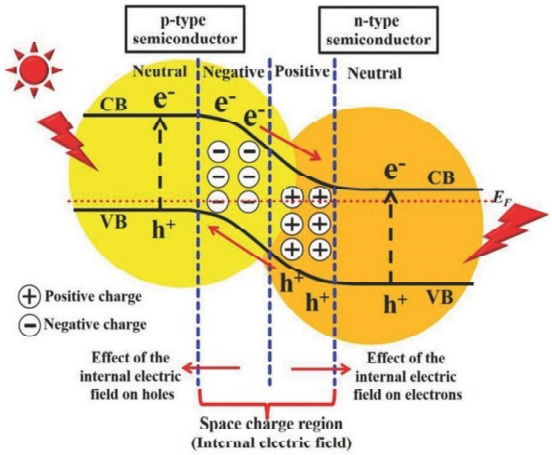


Figure: 9 p-n type heterojunction [48]

Hua et al [53] constructed $La_2Ti_2O_7/In_2S_3$ composite photocatalyst by electrostatic self-assembly of $La_2Ti_2O_7$ which is a p-type semiconductor and $In_2S_3$ which is an n-type semiconductor. There is a strong Coulomb static force between the negatively charged $In_2S_3$ and the positively charged $La_2Ti_2O_7$ in DMF, which makes the two materials tightly combined. $La_2Ti_2O_7$ and $In_2S_3$ have the best photocatalytic hydrogen production when the mass ratio is 7.5:1.0, which is 3.5 times the original $In_2S_3$ hydrogen production (Figure 10a). $In_2S_3$ and $La_2Ti_2O_7$ with different semiconductor types in order to balance the Fermi energy level will cause band bending and provide an additional electric field (Figure 10b). The p-n heterojunction composite photocatalyst can improve the photocatalytic performance by providing an additional electric field and thus by accelerating the electron hole migration of the heterojunction.

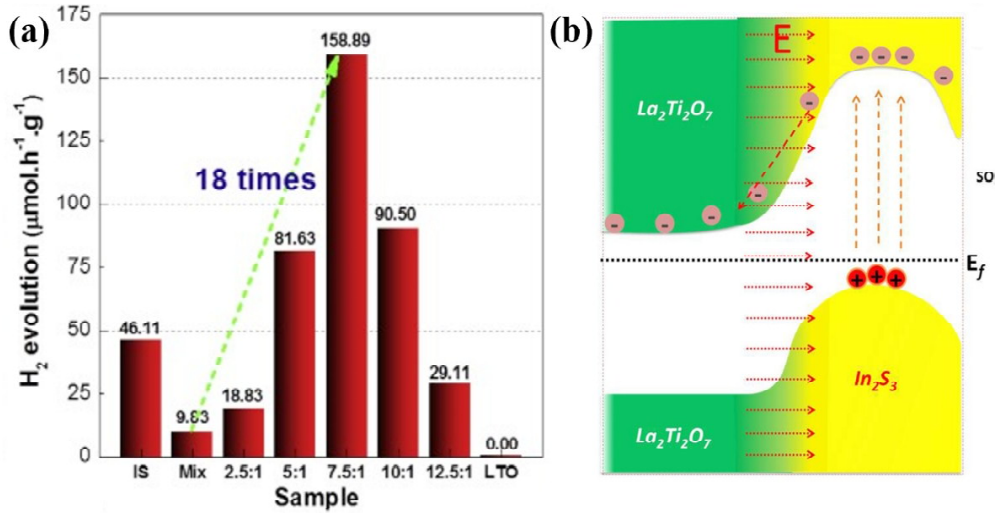


Figure: 10 (a) The average hydrogen production rate of different samples, "Mix" represents the physical mixture of $La_2Ti_2O_7$ and $In_2S_3$ (mass ratio 7.5:1.0), "LTO" represents $La_2Ti_2O_7$; (b) $La_2Ti_2O_7/In_2S_3$ nanosheet heterojunction energy Belt structure model [53]

Wang et al[54] synthesized $SnS_2/In_2S_3$ p-n heterojunction using a one-pot hydrothermal method for photocatalytic reduction of $Cr^{6+}$ to $Cr^{3+}$. The $Cr^{6+}$ photocatalytic reduction efficiency of 15%$SnS_2/In_2S_3$ is 3 times and 67 times that of pure $In_2S_3$ and $SnS_2$, respectively (Figure 11a). It was found that the sample can reduce $Cr^{6+}$ under the condition of ph less than 11, which provides a way to reduce $Cr^{6+}$ under alkaline conditions. Electron spin resonance (ESR) detection was also carried out to understand the migration path of photogenerated electrons, and finally the heterojunction type was p-n type semiconductor in type II (Figure 11b).

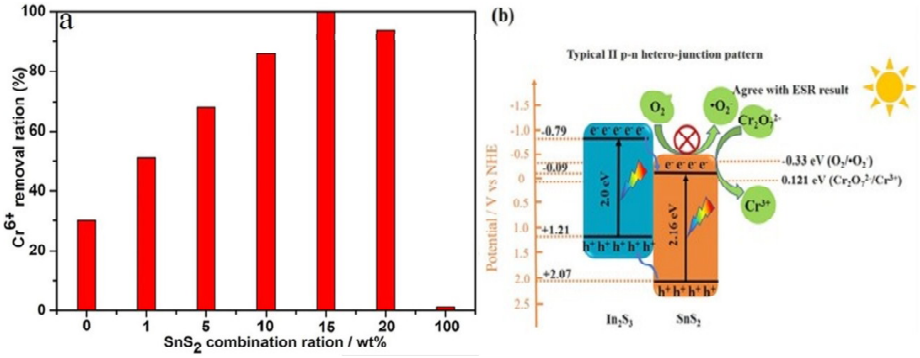


Figure: 11(a) Photoreduction efficiency of $In_2S_3$, $SnS_2$ and $SnS_2/In_2S_3$ heterostructures for $Cr^{6+}$ reduction; (b) Schematic diagram of electron transfer path in composite system. Type II p-n heterojunction [54]

### *3.9 $In_2S_3$-based Z-type heterojunction*

Although the first three types of heterojunctions have improved the separation of electrons and holes to varying degrees, they are all transferred to the relatively lower conduction band and valence band positions after they are excited by light. The redox ability of semiconductor heterojunctions has been weakened. The advantage of Z-type heterojunctions (as shown in Figure 12) is that on the basis of type II heterojunctions, electrons accumulated in relatively positive conduction band positions are directly transferred to relatively relatively high conduction bands. At the negative valence band position, the electron holes react in the more positive or negative valence band and conduction band position, retaining the stronger redox ability of the two semiconductors [48].

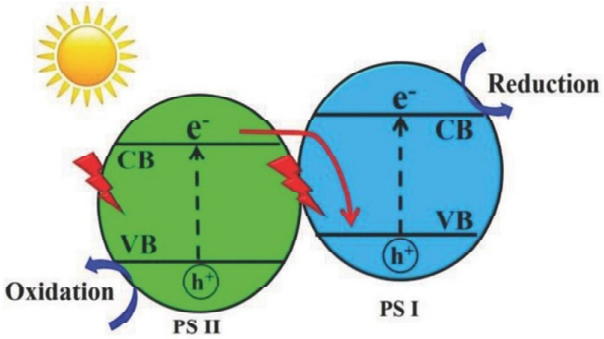


Figure: 12Z-type heterojunction [48]

Zhang et al [55] reported a ternary Z-type heterojunction photocatalyst prepared from graphene, $WO_3$ and $In_2S_3$. The $In_2S_3/WO_3/rGO$ photocatalyst prepared by the one-pot hydrothermal method combines rod-shaped $WO_3$ and flake-shaped $In_2S_3$ on graphene. As shown in Figure 13a, the photoexcited electrons in the conduction band of $WO_3$ are transferred to the valence band of $In_2S_3$, which makes the $In_2S_3/WO_3/rGO$ photocatalyst retain the high conduction band position of $In_2S_3$ and lower $WO_3$ compared to pure $In_2S_3$ and $WO_3$. The position of the valence band makes it have strong redox ability. As a result, when the molar ratio of $In_2S_3$ to $WO_3$ is 1:1, $In_2S_3/WO_3/rGO$ has the highest visible light photocatalytic activity, and the hydrogen production performance reaches 1524 $\mu mol \cdot g^{-1} \cdot h^{-1}$ (Figure 13b). The rGO nanosheets act as an effective charge linker and transporter in the $In_2S_3/WO_3/rGO$ ternary nanocomposite, which contributes to the good distribution of $In_2S_3$ and $WO_3$ on the body and effective contact on graphene. The Z-type heterostructure also improves the separation rate of electrons and holes.

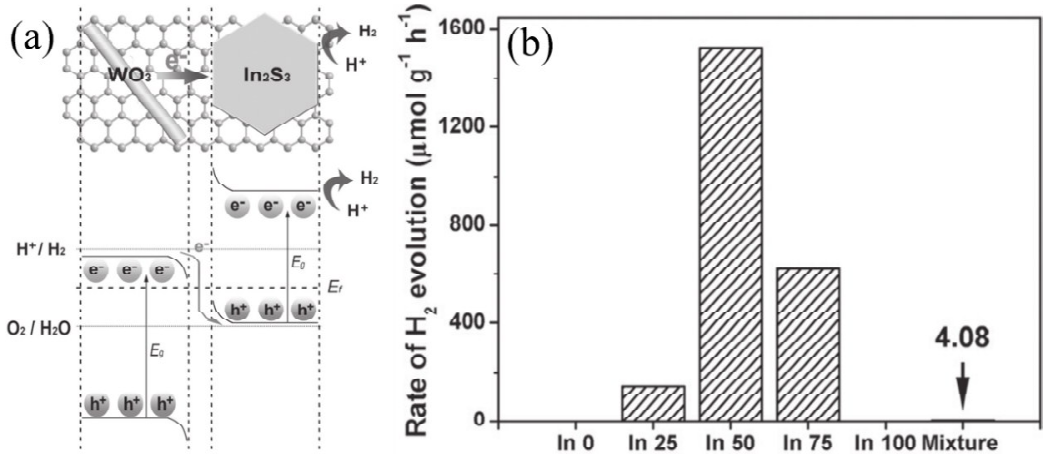


Figure: 13 (a) A model of $In_2S_3/WO_3/rGO$ tertiary nanocomposite as a photocatalyst of the Z scheme (top), with a schematic energy diagram for photocatalytic water splitting (bottom); (b) In 0 under visible light irradiation , In 25, In 50, In 75, In 100 nanocomposites and the $H_2$ precipitation rate of the mixture of $In_2S_3$ nanosheets and $WO_3$ nanorods.[55]

Hu et al [56] used a hydrothermal method to prepare the $In_2S_3/BiOBr$ heterojunction for the degradation experiment of the organic dye Rhodamine B, by changing the content of $In_2S_3$ to achieve the best degradation efficiency. Compared with the nanosheets of pure BiOBr, the prepared composite material presents a nanoflower structure with a diameter of about 4ìm (Figure 14a-b). The degradation effect of rhodamine B is 4.75 times and 11.26 times that of pure BiOBr and $TiO_2$ P25 catalysts (Figure 14c). As shown in Figure 14d, through the capture experiment to study the active free radicals in the photocatalytic process, it is found that superoxide radicals and holes are the free radicals that play a major role in the photocatalytic process. In addition, the increase in superoxide radicals measured by the measured ESR under light indicates that the type of heterojunction is a Z-type heterojunction (Figure 14e).

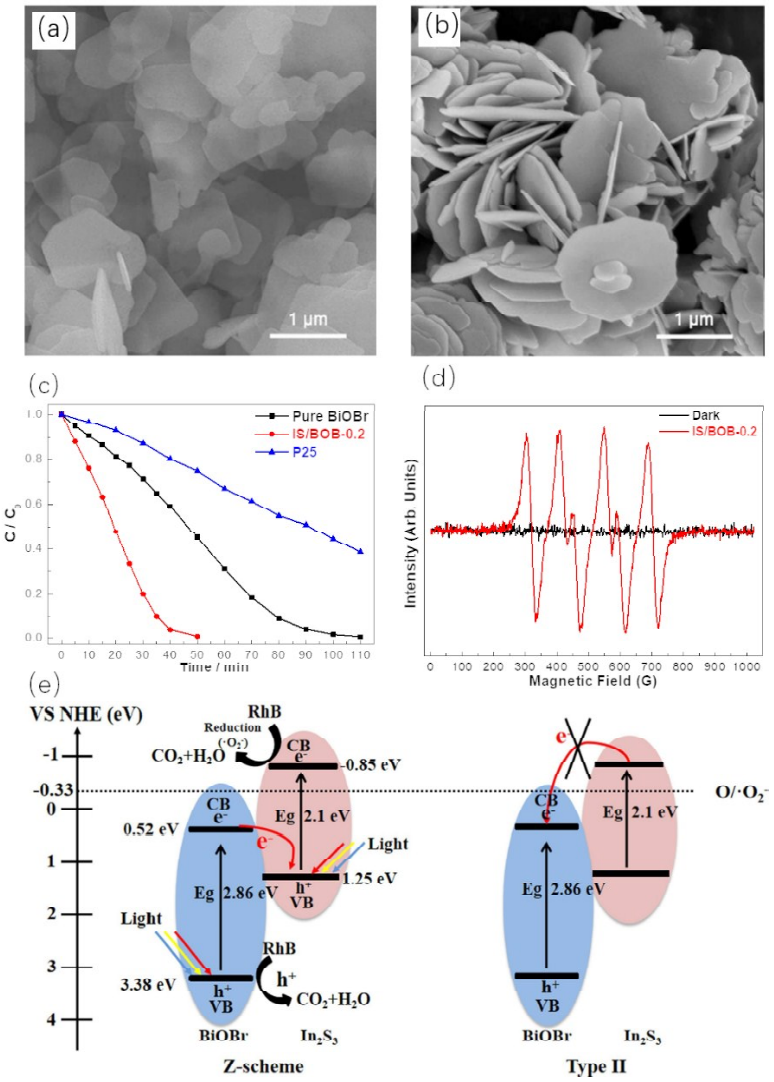


Figure: 14FESEM images of the prepared samples: (a) pure BiOBr, (b) $In_2S_3$/BiOBr-0.2; (c) photodegradation curve of RhB dye; (d) trapping experiment of $In_2S_3$/BiOBr-0.2; (e) Schematic diagram of the photocatalytic process of $In_2S_3$/BiOBr composite [56]

## 4. Conclusions and perspectives

In this review, the advantages of $In_2S_3$ when used as photocatalytic hydrogen production materials are discussed. $In_2S_3$ itself is non-toxic, coupled with excellent structure and optical advantages, so that it has an extremely broad application prospect in photocatalysis. The suitable narrow band gap (2.0eV-2.3eV) makes it possible to become a semiconductor photocatalyst. After absorbing enough light energy, the electrons in the valence band obtain enough energy to undergo transition and transfer to the conduction band. The electrons in the conduction band and the holes in the valence band are transferred to the surface of the material for reduction and oxidation respectively.

reaction. Even though the photocatalytic performance of $In_2S_3$ itself is superior, it still has some problems, such as the photocorrosion of the photocatalyst itself and the recombination of photogenerated electron-hole pairs during the photocatalytic reaction. In order to further improve the photocatalytic hydrogen production capacity of $In_2S_3$, you can adjust the morphology of $In_2S_3$ (such as 0D nanoparticles, 1D nanowires, nanorods, 2D nanosheets, 3D nanoflowers, etc.), and you can also use A method of recombining with other semiconductor materials to produce a heterojunction. However, even if the photocatalytic performance of $In_2S_3$ is optimized through the above methods, its research on photocatalytic hydrogen production still faces various challenges.

The following will talk about the problems of $In_2S_3$ in the direction of photocatalytic hydrogen production and possible better research directions from several directions. As an excellent optical device material, $In_2S_3$ is widely used in the application of photoelectric catalytic hydrogen production only in terms of the preparation of high-efficiency and clean hydrogen energy. However, the research on hydrogen production through the catalytic reaction of light energy is relatively small so far. . Combining $In_2S_3$ with some new materials for heterojunction may be a very promising research direction, such as black phosphorus, titanium carbide ($Ti_3C_2$) in Mxene materials and so on. The elaboration of the photocatalytic mechanism of $In_2S_3$ is not comprehensive at present. It is reflected in the transfer mechanism of photogenerated carriers, as well as the dynamics and thermodynamics of the semiconductor surface. More theoretical calculations and atomic research are needed.

## *Reference*

[1] R. Bariki, D. Majhi, K. Das, A. Behera, B.G. Mishra, Facile synthesis and photocatalytic efficacy of UiO-66/$CdIn_2S_4$ nanocomposites with flowerlike 3D-microspheres towards aqueous phase decontamination of triclosan and H2 evolution, Applied Catalysis B: Environmental, 270 (2020)118882.

[2] P. Lian, Y. Dong, Z.-S. Wu, S. Zheng, X. Wang, W. Sen, C. Sun, J. Qin, X. Shi, X. Bao, Alkalized $Ti_3C_2$ MXene nanoribbons with expanded interlayer spacing for high-capacity sodium and potassium ion batteries, Nano Energy, 40 (2017) 1-8.

[3] Waheed Iqbal, Bocheng Qiu, Qiaohong Zhu, Mingyang Xing, J. Zhang, Self-Modified Breaking Hydrogen Bonds to Highly, Applied Catalysis B: Environmental, 232(2018)306-313.

[4] Bo Chai, Tianyou Peng, P. Zeng, J. Mao, Synthesis of floriated $In_2S_3$ decorated with $TiO_2$ nanoparticles for efficient photocatalytic hydrogen production under visible light, Journal of Materials Chemistry, 38(2011) 14587–14593.

[5] F. AKIRA;, K. HONDA, Electrochemical Photolysis of Water at a Semiconductor Electrode, Nature, 238 (1972) 37-38.

[6] H. Tsuji, N. Sakai, H. Sugahara, Y. Gotoh, J. Ishikawa, Silver negative-ion implantation to sol–gel $TiO_2$ film for improving photocatalytic property under fluorescent light, Nuclear Instruments and Methods in Physics Research Section B: Beam Interactions with Materials and Atoms, 237(2005) 433-437.

[7] Xiaobo Chen, Shaohua Shen, Liejin Guo, S.S. Mao, Semiconductor-based Photocatalytic Hydrogen Generation, Chemical Reviews, 110 (2010) 6503-6570.

[8] G.M. Tomboc, B.T. Gadisa, J. Joo, H. Kim, K. Lee, Hollow Structured Metal Sulfides for Photocatalytic Hydrogen Generation, ChemNanoMat, 6 (2020) 850-869.

[9] S. Chandrasekaran, L. Yao, L. Deng, C. Bowen, Y. Zhang, S. Chen, Z. Lin, F. Peng, P. Zhang, Recent advances in metal sulfides: from controlled fabrication to electrocatalytic, photocatalytic and photoelectrochemical water splitting and beyond, Chem Soc Rev, 48 (2019) 4178-4280.

[10] J. Tan, M. Yu, Z. Cai, X. Lou, J. Wang, Z. Li, MOF-derived synthesis of MnS/$In_2S_3$p-n heterojunctions with hierarchical structures for efficient photocatalytic $CO_2$ reduction, J Colloid Interface Sci, 588 (2021) 547-556.

[11] A. Davoodi, M. Maddahfar, M. Ramezani, Application of mercaptoacetic acid as a capping agent, solvent, and precursor to fabricate In2S3 nanostructures, Journal of Industrial and Engineering Chemistry, 22 (2015) 368-372.

[12] W. Sheng, Y. Song, M. Dou, J. Ji, F. Wang, Constructing 1D hierarchical heterostructures of $MoS_2$/$In_2S_3$ nanosheets on CdS nanorod arrays for enhanced photoelectrocatalytic $H_2$ evolution, Applied Surface Science, 436 (2018) 613-623.

[13] H. Xu, Y. Wang, X. Dong, N. Zheng, H. Ma, X. Zhang, Fabrication of $In_2O_3$/$In_2S_3$ microsphere heterostructures for efficient and stable photocatalytic nitrogen fixation, Applied Catalysis B: Environmental, 257 (2019)117932-117941.

[14] C. Wei, W. Guo, J. Yang, H. Fan, J. Zhang, W. Zheng, Facile solvothermal synthesis of 3D flowerlike â-$In_2S_3$ microspheres and their photocatalytic activity performance, RSC Adv., 4 (2014) 50456-50463.

[15] Y. Pi, S. Jin, X. Li, S. Tu, Z. Li, J. Xiao, Encapsulated MWCNT@MOF-derived $In_2S_3$ tubular heterostructures for boosted visible-light-driven degradation of tetracycline, Applied Catalysis B: Environmental, 256 (2019)117832.

[16] Marie Buffière, Nicolas Barreau3, Guy Brammertz, S. Sahayaraj, M.M. , J. Poortmans, Development of Co-evaporated $In_2S_3$ Buffer Layer for Cu2ZnSnSe4 Thin Film Solar Cells, Institute of Electrical and Electronics Engineers, 42(2015)1-4.

[17] J. Li, Y. Ma, Z. Ye, M. Zhou, H. Wang, C. Ma, D. Wang, P. Huo, Y. Yan, Fast electron transfer and enhanced visible light photocatalytic activity using multi-dimensional components of carbon quantum dots@3D daisy-like $In_2S_3$/single-wall carbon nanotubes, Applied Catalysis B: Environmental, 204 (2017) 224-238.

[18] R. Bayon , J. Herrero, Structure and morphology of the indium hydroxy sulphide thin films, Applied Surface Science, 158 (1999) 49-57.

[19] X. Lai, F. Zhu, Y. Wu, R. Huang, X. Wu, Q. Zhang, K. Yang, S. Qin, New high-pressure polymorph of $In_2S_3$ with defect $Th_3P_4$-type structure, Journal of Solid State Chemistry, 210(2014) 155-159.

[20] Y. Sharma, P. Srivastava, Electronic, optical and transport properties of á-, â- and ã-phases of spinel indium sulphide: An ab initio study, Materials Chemistry and Physics, 135 (2012) 385-394.

[21] J. Zhang, H. Wang, X. Yuan, G. Zeng, W. Tu, S. Wang, Tailored indium sulfide-based materials for solar-energy conversion and utilization, Journal of Photochemistry and Photobiology C: Photochemistry Reviews, 38 (2019) 1-26.

[22] W. Wang, W. Zhu, L. Zhang, A facile preparation and visible light-induced photocatalysis of indium sulfide superstructure, Research on Chemical Intermediates, 35 (2009) 761-767.

[23] C. Huang, Y. Hong, X. Yan, L. Xiao, K. Huang, W. Gu, K. Liu, W. Shi, Carbon quantum dot decorated hollow $In_2S_3$ microspheres with efficient visible-light-driven photocatalytic activities, RSC Advances, 6 (2016) 40137-40146.

[24] B. Ma, M. Yue, P. Zhang, S. Li, R. Cong, W. Gao, T. Yang, Tetragonal â-$In_2S_3$: Partial ordering of $In^{3+}$ vacancy and visible-light photocatalytic activities in both water and nitrate reduction, Catalysis Communications, 88 (2017) 18-21.

[25] P. Ghaderi Sheikhi abadi, M. Salavati-Niasari, F. Davar, Hydrothermal synthesis, characterization and optical properties of 3D flower like indium sulfide nanostructures, Superlattices and Microstructures, 53 (2013) 76-88.

[26] C. D. Lokhande*, A. Ennaoui, P.S. Patil1, M. Giersig, K. Diesner, M.M. , H. Tributsch, Chemical bath

deposition of indium sulphide thin ®lms: preparation and characterization, Thin Solid Films 340 (1999) (1999) 18-23.

[27] H. Cui, S. Dong, K. Wang, M. Luan, T. Huang, Synthesis of a novel Type-II $In_2S_3$/$Bi_2MoO_6$ heterojunction photocatalyst: Excellent photocatalytic performance and degradation mechanism for Rhodamine B, Separation and Purification Technology, 255 (2021)117758.

[28] X. Fu, X. Wang, Z. Chen, Z. Zhang, Z. Li, D.Y.C. Leung, L. Wu, X. Fu, Photocatalytic performance of tetragonal and cubic â-$In_2S_3$ for the water splitting under visible light irradiation, Applied Catalysis B: Environmental, 95 (2010) 393-399.

[29] G. Liu, X. Jiao, Z. Qin, D. Chen, Solvothermal preparation and visible photocatalytic activity of polycrystalline â-$In_2S_3$nanotubes, CrystEngComm, 13 (2011) 182-187.

[30] W. Huang, L. Gan, H. Yang, N. Zhou, R. Wang, W. Wu, H. Li, Y. Ma, H. Zeng, T. Zhai, Controlled Synthesis of Ultrathin 2D â $In_2S_3$ with Broadband Photoresponse by Chemical Vapor Deposition, Advanced Functional Materials, 27 (2017)1702448-1702456.

[31] X. Yang, C.Y. Chan, H.T. Xue, J. Xu, Y.-B. Tang, Q. Wang, T.L. Wong, C.-S. Lee, One-pot synthesis of graphene/$In_2S_3$ nanoparticle composites for stable rechargeable lithium ion battery, CrystEngComm, 15 (2013)6578-6584.

[32] Z. Zhang, Y. Tang, C. Liu, L. Wan, Fabrication of $In_2S_3$ nanoparticle decorated $TiO_2$ nanotube arrays by successive ionic layer adsorption and reaction technique and their photocatalytic application, J Nanosci Nanotechnol, 14 (2014) 4170-4177.

[33] X. Xie, G. Shen, Single-crystalline $In_2S_3$ nanowire-based flexible visible-light photodetectors with an ultra-high photoresponse, Nanoscale, 7 (2015) 5046-5052.

[34] X. H. Sun1, and Boon K. Teo3, Zero-Dimensional Nanodots on One-Dimensional Nanowires: Reductive Deposition of Metal Nanoparticles on Silicon Nanowires, Journal ofCluster Science,15 (2004) 119-224.

[35] M. Zervos, P. Papageorgiou, A. Othonos, High yield–low temperature growth of indium sulphide nanowires via chemical vapor deposition, Journal of Crystal Growth, 312 (2010) 656-661.

[36] M. Afzaal, M.A. Malik, P. O'Brien, Indium sulfide nanorods from single-source precursor, Chem Commun, (2004) 334-335.

[37] Y. Chen, G. Tian, Q. Guo, R. Li, T. Han, H. Fu, One-step synthesis of a hierarchical $Bi_2S_3$ nanoflower\$In_2S_3$ nanosheet composite with efficient visible-light photocatalytic activity, CrystEngComm, 17 (2015) 8720-8727.

[38] M. Li, X. Tu, Y. Wang, Y. Su, J. Hu, B. Cai, J. Lu, Z. Yang, Y. Zhang, Highly Enhanced Visible-Light-Driven Photoelectrochemical Performance of ZnO-Modified $In_2S_3$ Nanosheet Arrays by Atomic Layer Deposition, Nanomicro Lett, 10 (2018) 45-57.

[39] M. Han, L. Yu, W. Chen, W. Wang, J. Jia, Fabrication and photoelectrochemical characteristics of $In_2S_3$ nano-flower films on $TiO_2$ nanorods arrays, Applied Surface Science, 369 (2016) 108-114.

[40] Li-Yong Chen, Zu-De Zhang, W.-Z. Wang, Self-Assembled Porous 3D Flowerlike â-$In_2S_3$ Structures: Synthesis, Characterization, and Optical Properties, J. Phys. Chem, C 2008, 112, (2008) 4117-4123.

[41] S. Yang, C.Y. Xu, B.Y. Zhang, L. Yang, S.P. Hu, L. Zhen, Ca(II) doped beta-$In_2S_3$ hierarchical structures for photocatalytic hydrogen generation and organic dye degradation under visible light irradiation, J Colloid Interface Sci, 491 (2017) 230-237.

[42] Y. Liu, M. Zhang, Y. Gao, R. Zhang, Y. Qian, Synthesis and optical properties of cubic $In_2S_3$ hollow nanospheres, Materials Chemistry and Physics, 101 (2007) 362-366.

[43] A.K. Nayak, S. Lee, Y. Sohn, D. Pradhan, Synthesis of $In_2S_3$ microspheres using a template-free and surfactant-less hydrothermal process and their visible light photocatalysis, CrystEngComm, 16 (2014)8064-8072.

[44] H. Pan, Principles on design and fabrication of nanomaterials as photocatalysts for water-splitting, Renewable and Sustainable Energy Reviews, 57 (2016) 584-601.

[45] R. Tong, K.W. Ng, X. Wang, S. Wang, X. Wang, H. Pan, Two-dimensional materials as novel co-catalysts for efficient solar-driven hydrogen production, Journal of Materials Chemistry A, 8 (2020) 23202-23230.

[46] M.J. Bierman, S. Jin, Potential applications of hierarchical branching nanowires in solar energy conversion, Energy & Environmental Science, 2 (2009)1005-1120.

[47] B. Sun, F. Shan, X. Jiang, J. Ji, F. Wang, One-pot synthesis of $MoS_2/In_2S_3$ ultrathin nanoflakes with mesh"shaped structure on indium tin oxide as photocathode for enhanced photo-and electrochemical hydrogen evolution reaction, Applied Surface Science, 435 (2018) 822-831.

[48] J. Low, J. Yu, M. Jaroniec, S. Wageh, A.A. Al-Ghamdi, Heterojunction Photocatalysts, Adv Mater, 29 (2017)1601694-1601714.

[49] X. Ma, C. Ren, H. Li, X. Liu, X. Li, K. Han, W. Li, Y. Zhan, A. Khan, Z. Chang, C. Sun, H. Zhou, A novel noble-metal-free $Mo_2C$-$In_2S_3$ heterojunction photocatalyst with efficient charge separation for enhanced photocatalytic H2 evolution under visible light, J Colloid Interface Sci, 582 (2021) 488-495.

[50] X. Yang, J. Xu, T. Wong, Q. Yang, C.S. Lee, Synthesis of $In_2O_3$-$In_2S_3$ core-shell nanorods with inverted type-I structure for photocatalytic $H_2$ generation, Phys Chem Chem Phys, 15 (2013) 12688-12693.

[51] M. Liu, P. Li, S. Wang, Y. Liu, J. Zhang, L. Chen, J. Wang, Y. Liu, Q. Shen, P. Qu, H. Sun, Hierarchically porous hydrangea-like $In_2S_3/In_2O_3$ heterostructures for enhanced photocatalytic hydrogen evolution, J Colloid Interface Sci, 587(2020)876-882.

[52] A. Prakash, M. Dan, S. Yu, S. Wei, Y. Li, F. Wang, Y. Zhou, $In_2S_3$/CuS nanosheet composite: An excellent visible light photocatalyst for $H_2$ production from H2S, Solar Energy Materials and Solar Cells, 180 (2018) 205-212.

[53] E. Hua, S. Jin, X. Wang, S. Ni, G. Liu, X. Xu, Ultrathin 2D type-II p-n heterojunctions $La_2Ti_2O_7/In_2S_3$ with efficient charge separations and photocatalytic hydrogen evolution under visible light illumination, Applied Catalysis B: Environmental, 245 (2019) 733-742.

[54] L. Wang, S.K. Karuturi, L. Zan, $SnS_2$-$In_2S_3$ p-n heterostructures with enhanced $Cr^{6+}$ reduction under visible-light irradiation, Applied Surface Science, 537 (2021)148063-148072.

[55] Q. Zhang, M. Luo, Y.P. Sun, Y. Liu, A. Cao, Efficient Z-scheme photocatalyst from simultaneous decoration of $In_2S_3$ nanosheets and $WO_3$ nanorods on graphene sheets, Nanotechnology, 27 (2016) 285602-285610.

[56] M. Hu, A. Yan, F. Li, F. Huang, J. Huang, Q. Cui, X. Wang, Z-scheme indium sulfide/bismuth oxybromide heterojunctions with enhanced visible-light photodegradation of organics, Applied Surface Science, 547 (2021)149234-149243.